SCIENCE CHINA
Technological Sciences

• Article •

December 2017 Vol.60 No.12: 1897–1902
doi: 10.1007/s11431-017-9080-5

Modulation of field emission by small AC signals

YANG Jin[1,2,5], ZHANG GengMin[1*], ZHOU HaiTao[3], WEI JinDi[1], CHEN YanHui[1] & SHEN ChengMin[4]

[1] *Key Laboratory for the Physics and Chemistry of Nanodevices and Department of Electronics, PekingUniversity, Beijing 100871, China;*
[2] *Academy for Advanced Interdisciplinary Studies, Peking University, Beijing 100871, China;*
[3] *AECC Beijing Institute of Aeronautical Materials, Beijing100095, China;*
[4] *Beijing National Laboratory of Condensed Matter Physics, Institute of Physics, Chinese Academy of Sciences, Beijing 100190, China;*
[5] *Chang'an Communication Technology Co., Ltd., Beijing 102209, China*

Received January 30, 2017; accepted June 1, 2017; published online August 4, 2017

In a microwave tube the energy of electrons in an electron beam, which are usually generated by a thermionic cathode, is modulated such that it is transformed into electromagnetic wave energy. In this paper, we modulated the field emission using AC signals. A field emission current with AC components was attained by adding a small AC voltage to a high extracting DC voltage. We observed two phenomena related to the AC components of the field emission current. First, when the DC component of the extracting voltage was low, the current measured in the circuit was dominated by the displacement current. Second, besides the fundamental frequency component, higher order harmonics were also observed in the field emission current.

field emission, AC modulation, displacement current, harmonics

Citation: Yang J, Zhang G M, Zhou H T, et al. Modulation of field emission by small AC signals. Sci China Tech Sci, 2017, 60: 1897–1902, doi: 10.1007/s11431-017-9080-5

1 Introduction

In a microwave tube, AC components must be introduced into an electron beam to convert the beam's energy into electromagnetic wave energy. In most microwave tubes, the electron beams are generated using thermionic cathodes. Meanwhile, cold cathodes are another potential electron beam source; the electrons can be extracted at room temperature from this type of source using high fields. Cold cathodes have advantages over thermionic cathodes, such as having a lower energy consumption, a smaller energy spread, a smaller volume, instant turn-on ability, and a good compatibility with modern microelectronic devices [1–6]. Therefore, some researchers are endeavoring to develop microwave tubes in which cold cathodes are used as the electron sources [7–9].

Over the last few decades, significant effort has been devoted to studying field emission in the search for ideal cold electron sources—most such research has been performed under DC voltages. However, some reports highlight a noteworthy difference of the field emission properties for cold cathodes under DC voltages and under pulsed voltages [10–12]. With regard to the use of cold cathodes in microwave tubes, Li et al. [13] simulated the modulation of an electron beam in a field-emission electron gun.

With these past studies in mind, we experimentally investigated how a time-varying voltage superposed on a DC voltage would modulate the field emission current. The results reported in this article demonstrate that a field emission current can be simultaneously obtained and modulated. The role of both the displacement current and the high-order harmonics caused by the nonlinear relationship between the field emission current and the applied voltage are also described herein.

*Corresponding author (email: zgmin@pku.edu.cn)

2 Experimental procedures

The field emission was measured for high DC voltages and for DC voltages modulated by small sinusoidal signals. Figure 1 shows diagrams of the circuits used for the measurements. As shown in Figure 1(a), a voltage source was used to provide a high negative voltage to the cathode. When a current in the circuit passes through a sampling resistor from the anode to the ground, it results in a voltage drop. This voltage drop across the sampling resistor was recorded using a data acquisition (DAQ) card. A microampere meter was also used in some measurements to monitor the currents directly.

As shown in Figure 1(b), the superposition of a small sinusoidal signal and the DC voltage was achieved by adding a small sinusoidal signal at the anode (with respect to the ground). A signal generator was used to output a sinusoidal voltage with a 10 V amplitude. This signal was fed into the circuit through a follower (an operational amplifier to guarantee a sufficient supply of power). The voltage drop across the sampling resistor between the anode and the output terminal of the follower was recorded with a DAQ card to determine the current in the circuit.

The field emitters in this study were made of vertically standing graphene sheets fabricated using the plasma enhanced chemical vapor deposition method (Figure 2). Details of the fabrication are available in ref. [14]. The field emission behavior of the samples was recorded in a laboratory-built ultrahigh vacuum system under a base pressure of 10^{-7} Pa.

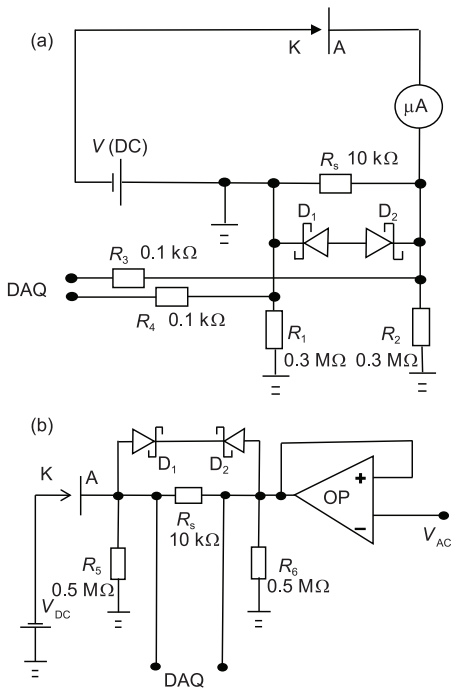

Figure 1 Diagram of the measurement circuits under (a) a DC high voltage and (b) a DC high voltage modulated by a small sinusoidal signal. K and A represent the cathode and the anode, respectively, while D_1 and D_2 are a pair of Zener diodes to protect the DAQ cards in case of an accidental discharge or short circuit between the cathode and anode. The two resistor pairs R_1/R_2 and R_5/R_6 are used to suppress the common-mode noise. R_3 and R_4 are both current-limiting resistors, while R_s is a sampling resistor and OP is a follower.

3 Results and discussion

3.1 Theoretical considerations

First, a pure DC voltage, denoted by V(DC), was applied to the cathode-anode gap; the circuit was in a steady state and the current was spatially continuous throughout the circuit, i.e., the current measured in the circuit was equal to the electron emission current from the cathode, denoted by I(DC).

Then, a DC voltage, denoted by $\overline{V}$, and a small AC component, denoted by $\tilde{V} = V_A\cos\omega_0 t = V_A\cos(2\pi f_0 t)$ (where t is time, V_A, ω_0 and f_0 are the amplitude, the angular frequency, and the frequency of $\tilde{V}$, respectively), were simultaneously applied across the cathode-anode gap. Under the voltage $V = \overline{V} + \tilde{V}$, a generalized continuity relationship replaced the continuity of the charge current. The cathode-anode gap was periodically charged and discharged, and this process produced a displacement current in the circuit. In this case, the current measured in the circuit was actually equal to the sum of the emissive current and the displacement current between the cathode and the anode. In other words, part of the current in the circuit was devoted to replenishing the emitted electrons from the cathode, and the other part was devoted to charging or discharging the cathode-anode condenser. This relationship can be expressed as

$$I_s = I_e + I_c, \tag{1}$$

where I_s is the current measured in the circuit (the subscript "s" stands for "sum"), I_e is the emissive current (the subscript "e" stands for "emissive"), and I_c is the displacement current, i.e., the charging current (the subscript "c" stands for "charging").

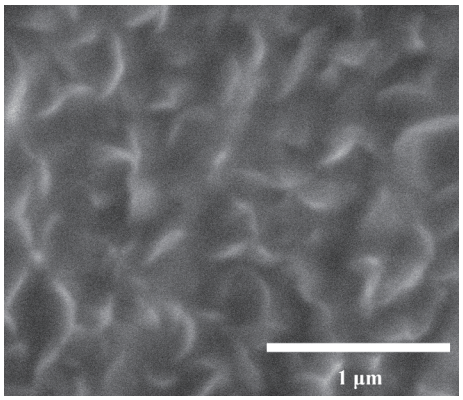

Figure 2 A scanning electron microscope image of the vertically standing graphene sheets.

During the generation of the emissive current I_e, $\overline{V}$ had the most significant role when it was sufficiently high and $\tilde{V}$ induced a modulation in I_e. The Taylor expansion of I_e around $\overline{V}$ can be performed as follows:

$$\begin{aligned} I_e &= I_e(\overline{V}+\tilde{V}) \\ &= I_e(\overline{V}) + I'_e(\overline{V})\tilde{V} + \frac{1}{2}I''_e(\overline{V})\tilde{V}^2 + \frac{1}{6}I'''_e(\overline{V})\tilde{V}^3 + \cdots \\ &= I_e(\overline{V}) + I'_e(\overline{V})V_A\cos\omega_0 t + \frac{1}{2}I''_e(\overline{V})V_A^2\cos^2\omega_0 t \\ &\quad + \frac{1}{6}I'''_e(\overline{V})V_A^3\cos^3\omega_0 t + \cdots, \end{aligned} \tag{2}$$

where $I'_e(\overline{V})$, $I''_e(\overline{V})$, and $I'''_e(\overline{V})$ are the first, second, and third order derivatives of I_e with respect to V at $V=\overline{V}$, respectively. Taking into consideration such relations as $\cos^2\omega_0 t = \frac{1+\cos 2\omega_0 t}{2}$ and $\cos^3\omega_0 t = \frac{3\cos\omega_0 t + \cos 3\omega_0 t}{4}$, eq. (2) can be written as a Fourier series of I_e:

$$I_e = I_{DC} + I_{f_0}\cos\omega_0 t + I_{2f_0}\cos 2\omega_0 t + I_{3f_0}\cos 3\omega_0 t + \cdots, \tag{3}$$

where

$$\begin{aligned} I_{DC} &= I_e(\overline{V}) + \frac{1}{4}I''_e(\overline{V})V_A^2 + \cdots, \\ I_{f_0} &= I'_e(\overline{V})V_A + \frac{1}{8}I'''_e(\overline{V})V_A^3 + \cdots, \\ I_{2f_0} &= \frac{1}{4}I''_e(\overline{V})V_A^2 + \cdots, \\ I_{3f_0} &= \frac{1}{24}I'''_e(\overline{V})V_A^3 + \cdots. \end{aligned} \tag{3a}$$

As shown in eq. (3), besides the DC component, the discrete frequency spectrum of I_e also contains the fundamental frequency (f_0) component as well as multiple fundamental frequency (nf_0, $n \geq 2$) components.

Besides modulating I_e, $\tilde{V}$ also generated I_c in the circuit. The equivalent circuit shown in Figure 3 was used for calculating I_c.

In Figure 3, R is the sum of all the resistances in the circuit, including those of the emitter and the emitter-substrate interface as well as the sampling resistor. C is the capacitance of the cathode-anode gap and $\frac{1}{j\omega C}$ is its complex impedance. The steady-state part of I_c is given by:

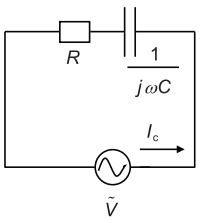

Figure 3 The equivalent circuit used for calculating I_c.

$$\begin{aligned} I_c &= Re\left(\frac{V_A e^{j\omega_0 t}}{R + \frac{1}{j\omega_0 C}}\right) \\ &= \frac{V_A}{R\sqrt{1+\frac{1}{R^2C^2\omega_0^2}}}\cos(\omega_0 t + \alpha) \\ &= I'_{f_0}\cos(\omega_0 t + \alpha), \end{aligned} \tag{4}$$

where

$$\begin{aligned} I'_{f_0} &= \frac{V_A}{R\sqrt{1+\frac{1}{R^2C^2\omega_0^2}}}, \\ \tan\alpha &= \frac{1}{\omega_0 RC}. \end{aligned} \tag{4a}$$

Unlike I_e, I_c is monochromatic. That is, it contains only f_0. Moreover, two characteristics of I_c can be used to further distinguish I_c from the f_0 component of I_e. First, the amplitude of the f_0 component of I_e, $I_{f_0} = I'_e(\overline{V})V_A + \frac{1}{8}I'''_e(\overline{V})V_A^3 + \cdots$, is independent of f_0, while the amplitude of I_c, $I'_{f_0} = \frac{V_A}{R\sqrt{1+\frac{1}{R^2C^2\omega_0^2}}}$, increases with f_0. Second, there is no phase difference between the f_0 component of I_e and $\tilde{V}$, while there is one between I_c and $\tilde{V}$, which is denoted by α in eq. (4).

Using eqs. (3) and (4), the expression of the current measured in the circuit is obtained as

$$\begin{aligned} I_s &= I_e + I_c \\ &= I_{DC} + \left[I_{f_0}\cos\omega_0 t + I'_{f_0}\cos(\omega_0 t + \alpha)\right] \\ &\quad + I_{2f_0}\cos 2\omega_0 t + I_{3f_0}\cos 3\omega_0 t + \cdots. \end{aligned} \tag{5}$$

3.2 DC field emission

First, we measured the field emission under pure DC voltages. As expected, I(DC) depended on V(DC) in an approximately exponential manner (here, all voltages and currents were measured from the anode to the cathode. Thus, V(DC), I(DC), and $\overline{V}$ are always positive).

The I(DC)-V(DC) relationship and the associated Fowler-Nordheim plot are presented in Figure 4(a). Moreover, the dependence of the derivative of I(DC) with respect to V(DC), $\frac{\mathrm{d}I(\mathrm{DC})}{\mathrm{d}V(\mathrm{DC})}$, on V(DC) is given in Figure 4(b). Here dV(DC) is approximated by a step in the V(DC) scan, ΔV(DC)=1.5 V, and the resulting increment in I(DC), ΔI(DC), is used as an approximation of dI(DC). As will be shown in the following section, the curve given by $\frac{\mathrm{d}I(\mathrm{DC})}{\mathrm{d}V(\mathrm{DC})} - V(\mathrm{DC})$ provides the necessary information to determine the frequency spectrum of the field emission current modulated by an AC voltage signal.

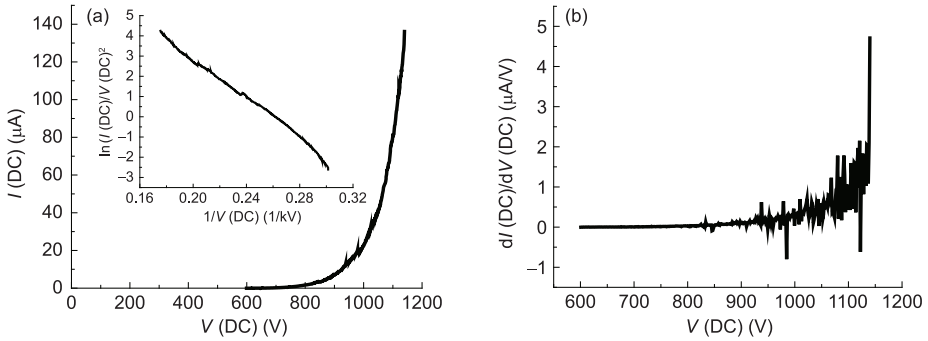

Figure 4 Field emission under pure DC voltages. (a) The I(DC)-V(DC) curve (inset: Fowler-Nordheim plot); (b) the dI(DC)/dV(DC)-V(DC) curve (the abrupt fluctuations at high voltages arise from the instability of the field emission).

3.3 Field emission modulated by AC signals

A small sinusoidal AC voltage ($\tilde{V} = V_A\cos\omega_0 t = V_A\cos(2\pi f_0 t)$) was superposed on the DC voltage ($\overline{V}$) so that the DC voltage and the AC voltage were simultaneously applied to the cathode-anode gap. For each measurement V_A was set at 10 V and f_0 was set to either 0.03 or 0.3 kHz. Four values of $\overline{V}$ were used: 600, 757, 1078, and 1130 V. As shown in Figure 4(a), a $\overline{V}$ of 600 V was still too low to extract any field emission. 757 and 1078 V were the turn-on and threshold voltages, respectively. Following common practice, the turn-on voltage was defined as the average voltage between the cathode and the anode for extracting a current density of 10 μA/cm^2. The threshold voltage was defined as the average voltage between the cathode and the anode for extracting a current density of 1 mA/cm^2 [15,16]. Under a $\overline{V}$ of 757 V, field emission began to emerge, although it was still rather weak. When $\overline{V}$ was raised to 1078 V, the field emission became sufficiently strong to be useful for some practical applications. When $\overline{V}$ was further raised to 1130 V, the field emission became even stronger.

The time domain waveforms and the fast Fourier transforms (FFTs) of the currents in the circuit (eq. (5)) under a voltage of $\overline{V}+\tilde{V}$ are shown in Figure 5. The waveforms in Figure 5(a) and (b) all assume an approximately sinusoidal shape. Under higher $\overline{V}$, the positions and the amplitudes of the waveforms are higher and larger, respectively. According to eqs. (3) and (3a), because $\tilde{V}$ is visibly smaller than $\overline{V}$, $I_e(\overline{V})$ dominates in the DC component, which determines the waveform position, and $I'_e(\overline{V})V_A$ dominates in the f_0 component, which determines the waveform amplitude at high $\overline{V}$. As shown in Figure 4, both $I_e(\overline{V})$ and $I'_e(\overline{V})$ should increase with $\overline{V}$ in an approximately exponential manner. The dependence of the waveform positions and the magnitudes on the values of $\overline{V}$ is echoed in the FFTs.

When $\overline{V}$ = 600 V, the DC components are very small for both f_0=0.03 and 0.3 kHz (Figure 5(c) and (d)). These negligibly small DC components are actually spurious signals caused by the small DC bias output from the DAQ cards. When $\overline{V}$ = 757 V, the DC components become observable but are still very small. When $\overline{V}$=1078 and 1130 V, in accordance with Figure 4(a), the DC components in the FFTs increased dramatically.

The dependence of I_{DC} on $\overline{V}$ described above is summarized in Figure 5(e). It is noticeable that the I_{DC}-$\overline{V}$ data points obtained with f_0=0.03 and 0.3 kHz almost coincide. This independence of I_{DC} on f_0 can be explained via eq. (3a), where I_{DC} is determined by only $\overline{V}$ and V_A and is independent of f_0.

The FFT of I_s at $\overline{V}$=600 V is dominated by the f_0 component (Figure 5(c) and (d)). According to Figure 4(a), when $\overline{V}$=600 V, the field emission was still almost nonexistent and the current measured in the circuit solely comprised the displacement current caused by $\tilde{V}$, i.e., $I_s \approx I_c$ and $I_{f_0} \ll I'_{f_0}$. That is, the currents measured in the circuit were almost exclusively caused by the cathode-anode condenser experiencing periodic charging and discharging driven by $\tilde{V}$. According to eq. (4), theoretically, I_c should be a harmonic current with a frequency identical to that of $\tilde{V}$.

At higher values of $\overline{V}$, i.e., 757, 1078, and 1130 V, the f_0 components, which are now dramatically dwarfed by the DC components, mainly result from $I'_e(\overline{V})$ (eq. (3a)). In contrast, I_c played a much smaller role. In accordance with Figure 4(b), the f_0 component increased with $\overline{V}$. As mentioned above, this increase is in agreement with the increase of the amplitudes of the time-domain waveforms with $\overline{V}$ shown in Figure 5(a) and (b).

The relationship between the f_0 components and $\overline{V}$ is summarized in Figure 5(f). When $\overline{V}$ is low, i.e., $\overline{V}$=600 or 757 V, I_{f_0} depends significantly on f_0. This behavior is quite different from that of I_{DC} (Figure 5(e)). When f_0=0.03 kHz, I_{f_0} was 0.34 μA for 600 V $\overline{V}$ and 0.37 μA for 757 V $\overline{V}$. When f_0=0.3 kHz, I_{f_0} rose to 3.9 μA for both of those values of $\overline{V}$. In contrast, for high values of $\overline{V}$, i.e., 1078 and 1130 V, the increase of f_0 from 0.03 to 0.3 kHz did not lead to an obvious change in I_{f_0}. That is, the f_0 component is

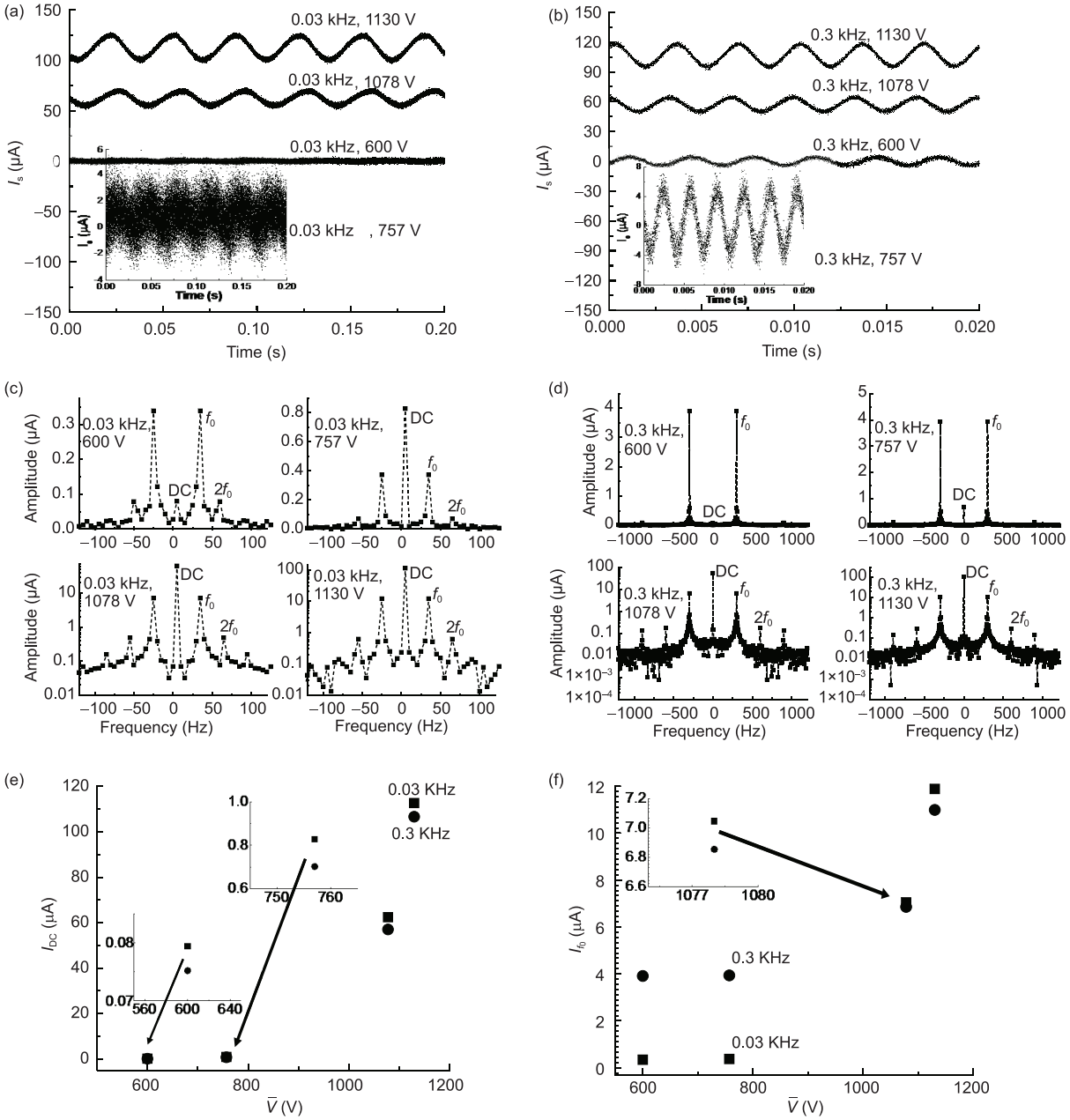

Figure 5 The waveforms and the FFTs of the currents measured in the circuit. (a) (b) The time-domain waveforms at f_0=0.03 and 0.3 kHz, respectively, and (c) (d) the corresponding FFTs; (e) (f) the dependence of I_{DC} and I_{f_0} on $\overline{V}$, respectively. In (c) (d), the ordinates of the two curves obtained under $\overline{V}$=1078 and 1130 V are logarithmic.

sensitive to f_0 at low $\overline{V}$ and insensitive to f_0 at high $\overline{V}$. This disparity in the I_{f_0}-f_0 relationship is evidence for a significant contribution from I_c at low applied voltages.

Field emission had not yet occurred when $\overline{V}$=600 V and was very weak when $\overline{V}$=757 V. Therefore, under low $\overline{V}$, I_s exclusively or mainly originated from I_c. As suggested in eq. (4a), the amplitude of I_c, I'_{f0}, is jointly determined by R, C, and f_0. In contrast, when $\overline{V}$ was increased to 1078 and 1130 V, I_e dominated in I_s and I_c was negligible in comparison with I_e, i.e., $I'_{f_0} \ll I_{f_0}$. According to eq. (3a), I_{f_0} is independent of f_0; thus the f_0 component of I_s did not change much under a voltage of $\overline{V}$ of 1078 and 1130 V.

In the FFT curves shown in Figure 5(c) and (d), besides the DC and f_0 components, components of multiple fundamental frequency, e.g. the $2f_0$ components, are also observable. The existence of these nf_0 ($n \geq 2$) components, which can be interpreted well using the Taylor expansion of I_e described by eq. (2), indicates that it may be possible to multiply the frequency of a source signal in a field emission process.

4 Conclusion

It is feasible to modulate the field emission at the same time as extracting it from a cold cathode by adding an AC signal to a high DC voltage. The displacement current dominates the current measured in the circuit under a low DC voltage and is negligible when the DC voltage is high. Because the field emission current depends on the applied voltage in an approximately exponential manner, high-order harmonics emerge in the frequency spectrum of the field emission current, indicating the possibility of frequency multiplication using field emission.

This work was supported by the Ministry of Science and Technology of China (Grant No. 2013CB933604), and the National Natural Science Foundation of China (Grant Nos. 51602300 & 61671022).

1 Mittal G, Lahiri I. Recent progress in nanostructured next-generation field emission devices. J Phys D-Appl Phys, 2014, 47: 323001
2 Xu N S, Huq S E. Novel cold cathode materials and applications. Mater Sci Eng-R-Rep, 2005, 48: 47–189
3 Chang C T, Chang Y T, Chih Y J, et al. Light-emitting illumination and field emission device of potassium hydroxide-doped electrochemically reduced graphene oxide. IEEE Trans Electron Devices, 2017, 64: 2251–2256
4 Li Y, Zhang Z, Zhang G, et al. Optimizing the field emission properties of ZnO nanowire arrays by precisely tuning the population density and application in large-area gated field emitter arrays. ACS Appl Mater Interfaces, 2017, 9: 3911–3921
5 Chen J, Yang B, Liu X, et al. Large field emission current and density from robust carbon nanotube cathodes for continuous and pulsed electron sources. Sci China Mater, 2017, 60: 335–342
6 Wei X Q, Li X, Liu W H, et al. Laser tuned field emission of the carbon nanotube arrays grown on an optical fiber. Sci China Tech Sci, 2014, 57: 1936–1940
7 Kim H J, Choi J J, Han J H, et al. Design and field emission test of carbon nanotube pasted cathodes for traveling-wave tube applications. IEEE Trans Electron Devices, 2006, 53: 2674–2680
8 Nation J A, Schachter L, Mako F M, et al. Advances in cold cathode physics and technology. Proc IEEE, 1999, 87: 865–889
9 Teo K B K, Minoux E, Hudanski L, et al. Microwave devices: Carbon nanotubes as cold cathodes. Nature, 2005, 437: 968–968
10 Zhang Y, Deng D, Zhu L, et al. Pulse field emission characteristics of vertical few-layer graphene cold cathode. IEEE Trans Electron Devices, 2014, 61: 1771–1775
11 Lei W, Zhang X B, Lou C G, et al. Very high field-emission current from a carbon-nanotube cathode with a pulse driving mode. IEEE Electron Device Lett, 2009, 30: 571–573
12 Yang J, Zhang G M. Behaviors of field emitters under pulsed voltages. Sci China Tech Sci, 2016, 59: 1777–1784
13 Li X X, Yuan X S, Zhang Y, et al. Theoretical research on electron beam modulation in a field-emission cold cathode electron gun. Chin Phys B, 2014, 23: 037901
14 Zhou H T, Yu N, Zou F, et al. Controllable preparation of vertically standing graphene sheets and their wettability and supercapacitive properties. Chin Phys B, 2016, 25: 096106
15 Lee C J, Lee T J, Lyu S C, et al. Field emission from well-aligned zinc oxide nanowires grown at low temperature. Appl Phys Lett, 2002, 81: 3648–3650
16 Bonard J M, Maier F, Stöckli T, et al. Field emission properties of multiwalled carbon nanotubes. Ultramicroscopy, 1998, 73: 7–15